Characterization of Electronic Properties in Complex Molecular Systems: Modeling of a Micropolarity Probe

Massimiliano Aschi,*,† Antonella Fontana,‡ Erika Maria Di Meo,‡ Costantino Zazza,§ and Andrea Amadei‖

Dipartimento di Chimica, Ingegneria Chimica e Materiali, Università di L'Aquila, via Vetoio (Coppito 1), 67010 L'Aquila, Italy; Dipartimento di Scienze del Farmaco, Università "G. d'Annunzio", Via dei Vestini 31, 66013 Chieti, Italy; Supercomputing Center for University and Research, CASPUR, via dei Tizii 6/b, 00185 Rome, Italy; and Dipartimento di Scienze e Tecnologie Chimiche, Università di Tor Vergata, via della Ricerca Scientifica 1, I-00133 Rome, Italy

Received: October 2, 2009; Revised Manuscript Received: December 21, 2009

Quantitative characterization of quantum states in complex molecular systems is a rather complicated task because of the necessity of maintaining the pure quantum definition of a state interacting with a configurationally complex molecular environment. Unfortunately, many of the "observables" that are of interest for a chemist, typically dealing with "complex objects", belong to the above class and their theoretical modeling may represent a hard task. In this respect, we have developed a new theoretical methodology, "perturbed matrix method", essentially based on the perturbation theory whose main aim is the characterization of the quantum states of a predefined portion of a complex molecular system, e.g., a solute, classically interacting with the environment, e.g., the solvent. This method has been used in this study to systematically characterize, for the first time and in conjunction with experimental observations, the intrinsic nature of pyrene whose vibrational and electronic states are highly sensitive to the nature of molecular environment. More precisely, pyrene shows a strong alteration of spectral intensities upon modification of polarity of the solvent. This property has been extensively used in many experimental studies and has been intepreted in the present study by characterizing pyrene electronic states as fluctuating states strictly connected to the polarity and the fluctuations of the surrounding medium. A correct theoretical modeling has been also obtained and commented for the vertical transitions in different media and also for the vibronic structure for the first transition in water.

1. Introduction

In the past years, theoretical and technological advancements have produced an impressive improvement of computational facilities providing a wide range of methodologies, economically and conceptually accessible for a huge number of researchers in different fields of molecular sciences. Electronic structure calculations[1] represent nowadays one of the most commonly used approaches by the physical−chemical community, allowing highly accurate description of systems with a large number of atoms, i.e., systems with an order of atoms of 10^2-10^3 and more.[2]

However, there is still a lot of work to do. As a matter of fact, modeling at the electronic level of systems with high configurational complexity is still challenging. In this case, the main problem is either practical and conceptual as the different observables to be modeled depend on processes occurring at different length, energy, and time scales. Computational tools typically employed for systems of such dimensions are classical simulations which, however, produce reliable results as far as transitions in quantum degrees of freedom do not take place. On the other hand, when the observables of interest explicitly involve quantum degrees of freedom, e.g., chemical reactions or spectral transitions, their modeling should be derived from statistical averages of genuine quantum states interacting with fluctuating perturbing environments. In the past years, our group has been focusing its efforts in this direction, producing a theoretical−computational methodology, perturbed matrix method (PMM),[3] whose main feature is to describe at electronic level a portion of a large molecular system maintaining the complexity of the overall system. Several applications, ranging from spectroscopic properties[4,5] to chemical reactions,[6,7] have been witnessing the rather good performance of the method. In a very recent application, PMM has also offered a new point of view of the perturbed electronic state which may be perceived in (classical) statistical−mechanical terms[8] similarly to more familiar concepts, such as for instance molecular structure, whose unique definition and relation with other chemical properties is possible only in the absence of conformational transitions, i.e., in the absence of any interaction with other molecules and/or an external thermal bath. In other words, whatever chemical property to be related to one or more quantum observables should also take into account these important, and typically nonstatic, interactions with the environment.

This latter aspect has been further investigated and exploited in the present study by applying PMM, in conjunction with molecular dynamics (MD) simulations, and experimental spectral measurements for characterizing perturbed electronic states of a benchmark molecule as pyrene. Pyrene (Figure 1) is a polycyclic aromatic hydrocarbon which, differently from solvatochromic molecules exhibiting either hypsochromic or bathochromic shift of their absorption spectral bands, undergoes

* To whom correspondence should be addressed. E-mail: aschi@caspur.it.
† Università di L'Aquila.
‡ Università "G. d'Annunzio".
§ Supercomputing Center for University and Research, CASPUR.
‖ Università di Tor Vergata.

10.1021/jp909465f
Published on Web 01/15/2010

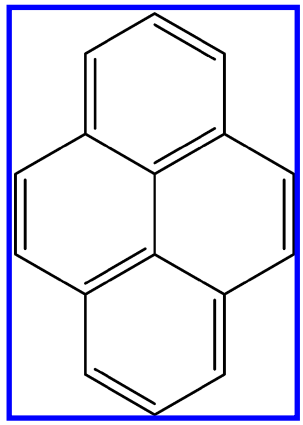

Figure 1. Pyrene structure.

sharp variations of spectral intensities (both absorption and emission spectra) depending on the polarity and the nature of the solvent. For this reason, it represents a widely used fluorescent probe for studying the molecular dynamics, the structural organization, and the polarity of assemblies that have defined hydrophobic environments.[9−13]

Such a peculiar property, beyond its practical importance is also of a great fundamental interest and its understanding is particularly important. Fluorescence response of pyrene has been explained by invoking a vibronic coupling between the first two electronic excited states,[14] but a systematic investigation of its perturbed electronic properties and their coupling with perturbing environment has never been attempted in the past. Such a problem, appearing in line with PMM features, has been addressed in the present study in which, using a joint application of experimental and computational methods, we have investigated the effect of five different media, namely water, acetonitrile, methanol, 1-palmitoyl-2-oleoylphosphatidylcholine (POPC) membrane, and hexane on the spectral (absorption) intensities of pyrene in the energy range 250−350 nm. The different solvents have been selected in order to span a relatively large repertoire of dielectric and chemical properties. The POPC membrane has been chosen because pyrene is widely used as a polarity probe for assemblies such as micelles and lipid vesicles, for example, to investigate the degree of water penetration[15] or the variations induced by the presence of a guest.[16] The present study is organized as follows. After a concise review of the theoretical framework and a more detailed description of experimental and computational methodologies, spectroscopic results and a theoretical analysis of the vertical absorption transitions will be presented. Finally, a semiquantitative evaluation of pyrene perturbed vibronic transitions will be also presented.

2. Experimental Section

2.1. Materials. 1-Palmitoyl-2-oleoyl-*sn*-glycero-3-phosphocholine (POPC) was purchased from Avanti Polar Lipids (Alabaster, AL). Pyrene, chloroform, acetonitrile, and methanol (Sigma-Aldrich) were used without further purification. Ultrapure Milli-Q water (Millipore Corp., model Direct-Q 3) with a resistivity of >18.2 MW cm was used to prepare all solutions.

2.2. Sample Preparation. Solutions of pyrene 2×10^{-6} M in H_2O, acetonitrile, and methanol were obtained from a pyrene stock solution in ethanol 2×10^{-3} M. Large unilamellar vesicles (LUV) were prepared evaporating to dryness by rotary evaporation at 40 °C 1 mL of a solution of POPC in chloroform. The obtained thin phospholipidic film, dried under vacuum for an additional 30 min, was kept at 4 °C at least for a night and then rehydrated with 5 mL of phosphate buffer saline (PBS, pH 7.40, 578 mOsm). The homogeneous dispersion of liposomes was achieved by extrusion (Lipex Biomembranes, Vancouver BC, Canada) through polycarbonate filters (Osmonics, pore size 200 nm). The final concentration of POPC in the diluted liposome suspension was 2.6 mM. Five micromilliliters of pyrene stock solution was added to the buffered liposomal suspension in order to obtain a final pyrene concentration of 2×10^{-6} M. We chose such a low pyrene concentration in order to avoid the formation of excimers. All the measurements were carried out at 25 ± 0.1 °C. The absorption measurements were performed on a Jasco V-550 UV−vis spectrophotometer from 230 to 350 nm.

3. Theoretical and Computational Section

3.1. MD Simulations. Molecular dynamics simulations were carried out by putting pyrene at the center of a rectangular box. Three different solvents were used, namely: single point charge[17] (SPC) water molecules at the typical density of 1000 kg/m^3, and methanol and acetonitrile at their typical liquid density of 782.2 kg/m^3.[18] In the case of membrane simulation, a fully hydrated and equilibrated POPC membrane[19] consisting of 128 POPC molecules and 4480 SPC water molecules was adopted. Lipid force field parameters were used as described by Berger et al.[20] The simulation was initiated by putting pyrene in the polar head region. For all the simulations the same protocol was adopted. Following an energy minimization and subsequent solvent relaxation, the systems were gradually heated from 50 to 300 K using short (20 ps) MD simulations. The trajectories in water, methanol, and acetonitrile were then propagated up to 10 ns in a NVT (300 K) ensemble using an integration step of 2.0 fs with the rototranslational constraint[21] applied to the solute. In the case of POPC, the trajectory was propagated up to 40.0 ns without rototranslational constraints. The temperature was kept constant at room temperature by the isokinetic temperature coupling,[22] and all bond lengths were constrained using LINCS algorithm.[23] Long-range electrostatics was computed by the particle mesh Ewald method[24] with 34 wave vectors in each dimension and a fourth-order cubic interpolation. Gromos force field[25] parameters were adopted. In the case of pyrene, atomic point charges were recalculated by the ESP procedure[26] using calculations with Becke's three-parameter exchange and the Lee, Yang, and Parr correlation functional (B3LYP)[27,28] and 6-311G(d) basis set. Atomic charges are reported in the Supporting Information.

3.2. Quantum Chemical and Perturbed Matrix Method Calculations. MD simulations previously described have been combined to PMM in order to provide the vertical absorption spectra of pyrene in the range 250−350 nm.

In the PMM procedure,[3−5] it is important to preventively select a part of the system, in this study pyrene, to be treated at electronic level (hereafter termed as quantum center, QC) with the rest of the system, in this study the solvent and/or the membrane, providing the perturbing electric field. Indicating with $\mathbf{r}_n$ the QC coordinates and with $\mathbf{x}$ the atomic coordinates of the perturbing environment, we can write the perturbed electronic Hamiltonian matrix as

$$\tilde{H}(\mathbf{r}_n, \mathbf{x}) = \tilde{H}^0(\mathbf{r}_n) + q_T V(\mathbf{r}_{com}, \mathbf{x})\tilde{I} + \tilde{Z}_1(E(\mathbf{r}_{com}, \mathbf{x}), \mathbf{r}_n) + \Delta U(\mathbf{r}_n, \mathbf{x})\tilde{I} \quad (1)$$

where $\tilde{H}^0(\mathbf{r}_n)$ is the unperturbed Hamiltonian matrix constructed using QC unperturbed basis set from quantum chemical (QM) calculations on the corresponding $\mathbf{r}_n$ coordinates. q_T is the total

charge of QC, while $V(\mathbf{r}_{com},\mathbf{x})$ and $E(\mathbf{r}_{com},\mathbf{x})$ are the electrostatic potential and field, respectively, acting step by step at the QC center of mass (termed as $\mathbf{r}_{com}$).

$\tilde{Z}_1$ is a perturbation energy matrix given by

$$\tilde{Z}_1(\mathbf{E}(r_{com},x),r_n) = -\mathbf{E}\cdot\langle\Phi_l^0|\hat{\boldsymbol{\mu}}|\Phi_{l'}^0\rangle \quad (2)$$

where Φ_1^0 are the unperturbed electronic Hamiltonian eigenfunctions and $\Delta U(\mathbf{r}_n,\mathbf{x})\tilde{I}$ approximates all the perturbation due to higher-order terms to simple short-range potential. Diagonalization of the perturbed electronic Hamiltonian (eq 1) produces a trajectory of perturbed eigenvalues and eigenvectors ($\mathbf{c}_i$) of QC. Perturbed eigenvectors can be used to evaluate whatever perturbed electronic property, in particular perturbed excitation energies and transition dipoles, $\boldsymbol{\mu}_{i,j}$, to be used for calculating the absorption spectra intensities, according to eq 3.

$$\boldsymbol{\mu}_{i,j} = c_i^T\langle\Phi_l^0|\hat{\mu}_x|\Phi_{l'}^0\rangle c_j\mathbf{i} + c_i^T\langle\Phi_l^0|\hat{\mu}_x|\Phi_{l'}^0\rangle c_j\mathbf{j} + c_i^T\langle\Phi_l^0|\hat{\mu}_x|\Phi_{l'}^0\rangle c_j\mathbf{k} \quad (3)$$

This is accomplished by using eqs 4 and 5 by considering a unitary radiation energy density per unit frequency

$$\varepsilon_{i,j}(\nu) = B_{i,j}(\nu)\rho(\nu)\frac{h\nu}{c} \quad (4)$$

$$B_{i,j} = \frac{|\boldsymbol{\mu}_{i,j}|^2}{6\varepsilon_0\hbar^2} \quad (5)$$

where $B_{i,j}$ is the Einstein coefficient, $\rho(\nu)$ is the probability density in the frequency space, and h and c are Planck's and speed of light constants. The perturbed transition dipoles squared lengths are obtained by averaging over the distribution of the corresponding frequency interval.[5]

Electronic structure calculations were performed, at the levels indicated in the next subsections, by using the Gaussian03[29] and Gamess US[30] packages.

4. Results and Discussion

4.1. Unperturbed Calculations. Application of PMM requires a preliminary evaluation of a proper set of electronic excited states characterizing the unperturbed basis set, Φ_l^0. In the case of gaseous pyrene, which has represented a benchmark molecule in the last years for the application of electronic structure theory, widespread amount of data can be found in the literature. Pyrene is a tetracyclic hydrocarbon belonging to D_{2h} point group whose gaseous absorption spectrum is characterized by a weak $S_0 \rightarrow S_1$ band at 369 nm corresponding to $1^1Ag \rightarrow 1^1B_{3u}$ (L_b) vertical transition and a more intense $S_0 \rightarrow S_2$ band at 322 nm assigned to the $1^1A_g \rightarrow 1^1B_{3\,g}$ (L_a) transition. The spectrum also shows three additional less intense and large peaks at slightly higher energies corresponding to vibronic transitions.[31] A second characteristic and intense band, the B-band at 265 nm,[32,33] is also accompanied by a vibronic structure. Although it is nowadays widely accepted that, even for the lowest vertical excited states a correct theoretical description cannot be achieved without the inclusion of electron dynamic correlation (e.g., multireference configuration interaction),[34,35] the possibility of using alternative and less expensive methods has obviously been extensively investigated in the past decades. Calculations within the Pariser−Parr−Pople (PPP) approximation[36] and other semiempirical methods[37,38] correctly reproduce the above absorption bands. Time-dependent density functional theory (TD-DFT) methods,[39] representing one of the most popular low-cost methods for these purposes, are usually found to underestimate the excitation energy of the states with dominant ionic character, i.e., S_2 in the case of pyrene, and none of the currently available functionals appear able to fully circumvent this limitation.[40]

In the view of this amount of information, we decided to evaluate the unperturbed basis set, i.e., Φ_l^0, using two alternative methods: ZINDO/6-311++g(d,p) using HF/6-311+g(d,p)-optimized geometry and TD-DFT making use of different functional and basis sets, namely B3LYP/cc-pVTZ, PBEPBE/6-31+g(d,p),[41] and VXSC/6-31+g(d,p),[42] on the corresponding optimized geometries. An additional set of calculations, carried out in particular for confirming the reliability of the ZINDO and TD-DFT dipole matrix elements, was also performed using the correlated equation of motion coupled cluster (EOM-CCSD) method[43] with 6-31g(d) basis set carried out on the corresponding HF/6-31g(d) optimized geometry. From ZINDO and TD-DFT, 13 states were evaluated; on the other hand only 6 states were calculated with EOM-CCSD method. The results for the transitions in the range 250−350 nm are reported in Table 1 whereas the corresponding geometries are collected in the Supporting Information.

Results in Table 1, in line with theoretical data present in the literature, show the rather good performance of ZINDO and confirm the limitations of the TD-DFT-B3LYP approach when the ordering of the first two excited states is considered. The additional functionals PBEPBE and VSXC, never tested in previous studies at this purpose, beyond the inversion of the first two transitions, systematically underestimate all the remaining energies. At the same time, the correlated ab initio approach EOM-CCSD, although correctly performing in the description of the sequence of the S_1 and S_2 states, overestimates the corresponding energies.

In the light of these findings we decided to apply PMM using, as unperturbed basis set, the ZINDO and TD-DFT-B3LYP excited states whose energies and transition moments should ensure a good reproduction of the essential physics of the system.

4.2. Experimental Data in Condensed Phase. Our measurements were performed at the lowest concentration of 10^{-6} mol dm^{-3} in order to avoid aggregation phenomena which are known to produce sharp effects on the absorption spectrum.[45]

Results reported in Table 2, in perfect agreement with the available literature data,[47] clearly indicate that the polarity of the medium (highlighted by both the dielectric constant and the I_1/I_3 indices), although leaving basically unaffected the position of the absorption maxima strongly affects the corresponding intensities. Corresponding spectra are also reported in Electronic Supporting Information.

Note that, based on the fact that the 261−271 nm intensity ratio essentially equals the 319−334 nm one, also the peak at 261 nm should be assigned as a vibronic transition.

From the data in the POPC bilayer, it appears that pyrene, once added to a liposomal suspension, tends to preferentially solubilize into the hydrophobic core of the bilayer, thus experiencing a relatively low polar environment as highlighted by the relatively high intensity of its bands. In this stage of the study, we are therefore in the position of addressing the numerical experiment to reproduce such spectral features and

TABLE 1: Comparison between Calculated and Experimental Vertical Transition Energies (nm) and Oscillator Strengths (in Parentheses) for Gaseous Pyrene

transition	B3LYP	PBEPBE	VSXC	EOM-CCSD	ZINDO	expt[a,b]
$S_0 \rightarrow S_1$	336 (0.25)	370 (0.22)	358 (0.24)	303 (0.0006)	351 (0.003)	369 (0.002)
$S_0 \rightarrow S_2$	330 (0.0004)	359 (0.0001)	345 (0.0002)	245 (0.38)	340 (0.48)	322 (0.33)
$S_0 \rightarrow S_3$	270 (0.25)	324 (0.00)	311 (0.00)	231 (0.00)	288 (0.00)	–
$S_0 \rightarrow S_4$	267 (0.00)	298 (0.18)	286 (0.20)	231 (0.00)	268 (0.00)	–
$S_0 \rightarrow S_5$	246 (0.00)	297 (0.00)	285 (0.00)	213 (0.00)	265 (0.93)	265 (0.35)

[a] Reference 44. [b] Reference 32.

TABLE 2: Absorption Maxima (nm) of Pyrene in the Investigated Media (Whose Dielectric Constants ε and I_1/I_3 Polarity Index[a] Are Reported in Parentheses) in the Range 230−350 nm[b]

water (ε 78.4; I_1/I_3 1.87)[c]	acetonitrile (ε 37.5, I_1/I_3 1.79)[c]	methanol (ε 32.7; I_1/I_3 1.35)[c]	POPC bilayer (ε 2 and ≈20;[d] I_1/I_3 0.82)[e]	hexane (ε 1.9; I_1/I_3 0.58)[c]
334* [**1.0**]	333* [3.4]	333* [4.0]	339* [3.7]	333* [4.2]
319 [0.7]	319 [2.3]	318 [2.7]	322 [2.0]	318 [2.9]
306 [0.3]	306 [1.0]	305 [1.1]	309 [0.7]	305 [1.3]
271* [1.0]	271* [3.3]	271* [3.7]	274* [3.1]	271* [4.1]
261 [0.7]	261 [2.0]	261 [2.3]	264 [1.6]	261 [2.7]
238* [1.9]	238* [3.4]	238* [3.9]	239* [3.6]	233* [4.0]

[a] The well-known Py scale for the solvent polarity had been established on the strong perturbation of the vibronic band intensities of pyrene. The solvent polarity dependence of pyrene's emission is expressed in terms of the intensity ratio, I_1/I_3, which are the intensities of bands I and III of the pyrene emission spectrum [$\lambda_{em}(I_1) = 375$ nm and $\lambda_{em}(I_3) = 384$ nm]; the larger the ratio, the more polar the medium. [b] The maximum intensity ratios with respect to the first transition in water (absorbance = 9750 $dm^3\ mol^{-1}\ cm^{-1}$, indicated in bold) are reported in brackets. The asterisk denotes a vertical transition. A maximum error of ±0.1 is estimated for the intensity ratios. [c] Reference 10. [d] The dielectric constants reported for the POPC bilayer correspond to the ones experimentally measured by means of the solvatochromic 2-anthroyl fluorophore [ref 45] for the hydrophobic and the hydrated interfacial region of egg-PC bilayers, respectively. [e] Reference 16.

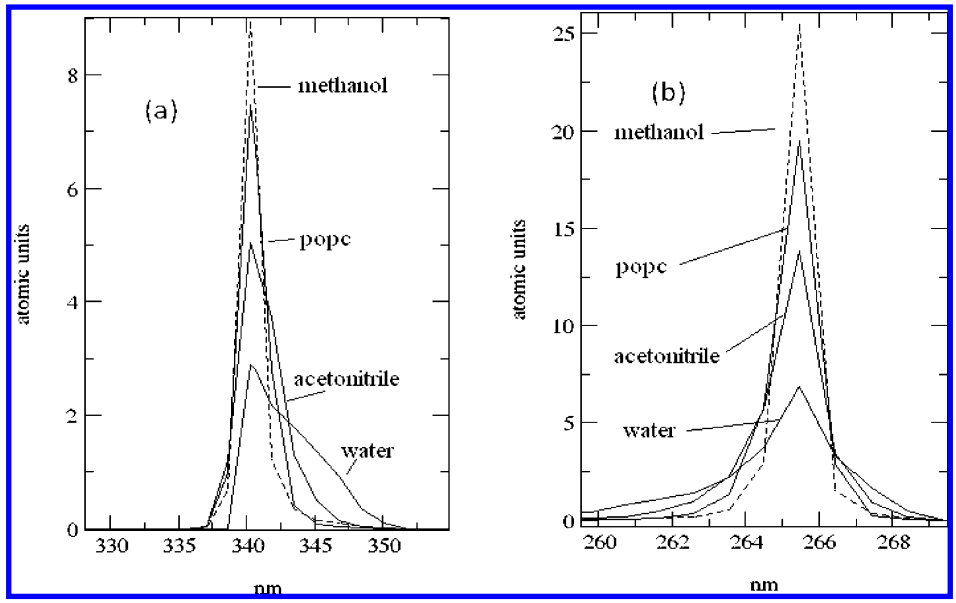

Figure 2. PMM-ZINDO absorption spectra in the range 300−350 nm (panel a) and 250−300 nm (panel b) in water, acetonitrile, methanol (dotted line), and POPC bilayer.

to provide some sort of interpretation. This will be described in the next section.

4.3. Theoretical Evaluation of Vertical Excitations in Condensed Phase. PMM, combined with MD simulations, was first applied for calculating vertical absorption energies of pyrene in the different solvents and within the POPC membrane. In the latter case, after a few hundreds of picoseconds pyrene was found to stably reside within the hydrophobic region, only seldom reaching the head polar groups. We must stress the fact that we were not interested in accurately spanning the equilibrium configurational space of POPC−membrane/pyrene system but, rather, to evaluate, if any, differential effects of pyrene relative position on its electronic properties. Further details concerning the results of the simulation can be found in the Supporting Information.

It is also important to remark that because of the dimension of the unperturbed basis set we limited our attention to the energy range up to 250 nm. Higher energy transitions would require a larger dimension of the electronic Hamiltonian operator to be used in PMM calculations.[4]

PMM-ZINDO and PMM-TD-DFT-B3LYP results are reported in Figure 2, a and b, respectively. In Table 3 the corresponding numerical values are also collected.

If we exclude the already remarked inversion of the two transitions obtained with TD-DFT-B3LYP, the experimental vertical energies are satisfactorily reproduced. A good internal agreement is also found comparing ZINDO and TD-DFT-B3LYP with the only relevant exception of the larger $S_0 \rightarrow S_5$ intensity obtained with ZINDO. Note that the two higher-energy transitions at 269 and 265 nm, obtained in both our numerical

TABLE 3: Vertical Absorption Maxima (nm) of Pyrene in Solution from PMM Calculations[a]

	water	acetonitrile	methanol	POPC bilayer
$S_0 \rightarrow S_1$ PMM-ZINDO	352 [0.12]	351 [0.19]	351 [0.20]	351 [0.18]
PMM-TDDFT	*335* [**1.0**]	*333* [2.2]	*333* [3.4]	*333* [3.3]
$S_0 \rightarrow S_2$ PMM-ZINDO	342 [**1.0**]	341 [2.0]	340 [3.6]	341 [2.5]
PMM-TDDFT	*329* [0.05]	*329* [0.12]	*328* [0.12]	*329* [0.14]
$S_0 \rightarrow S_3$ PMM-ZINDO	285 [0.02]	287 [0.05]	286 [0.02]	287 [0.05]
PMM-TDDFT	*279* [0.09]	*280* [0.13]	*280* [0.07]	*280* [0.13]
$S_0 \rightarrow S_4$ PMM-ZINDO	269 [1.7]	269 [2.6]	269 [1.1]	269 [1.0]
PMM-TDDFT	*268* [1.1]	*267* [1.0]	*268* [1.5]	*267* [1.5]
$S_0 \rightarrow S_5$ PMMZINDO	265 [1.8]	265 [5.5]	265 [7.8]	265 [6.0]
PMM-TDDFT	*266* [1.0]	*266* [2.0]	*267* [2.9]	*266* [2.7]

[a] The relative maxima intensities with respect to the first intense transition in water (absorbance = 2.5 atomic units for ZINDO and absorbance = 1.2 atomic units for *TD-DFT-B3LYP*, indicated in bold) are reported in brackets.

TABLE 4: Deviation of the Perturbed Transition Dipole Square Length, Corresponding to the Spectrum Maximum with Respect to the Unperturbed Value[a]

	water	acetonitrile	methanol	POPC bilayer
$S_0 \rightarrow S_2$ PMM-ZINDO	-0.169 ± 0.007	-0.007 ± 0.002	-0.001 ± 0.001	-0.004 ± 0.002
$S_0 \rightarrow S_1$ PMM-TD-DFT	-0.171 ± 0.008	-0.008 ± 0.002	-0.001 ± 0.001	-0.005 ± 0.002
$S_0 \rightarrow S_5$ PMM-ZINDO	-0.122 ± 0.007	-0.009 ± 0.003	-0.002 ± 0.002	-0.006 ± 0.003
$S_0 \rightarrow S_5$ PMM-TD-DFT	-0.131 ± 0.007	-0.009 ± 0.003	-0.002 ± 0.002	-0.006 ± 0.003

[a] Atomic units are used.

procedures, presumably merge in the band experimentally observed at about 271 nm.

First of all, it is important to briefly comment on the absence of any energy shift upon solvent (polarity) variation. This may be explained by the fact that pyrene unperturbed and perturbed dipoles of the states S_0, S_1, S_2, and S_3 do not undergo any appreciable deviation from zero. The only difference observed when we pass gas phase to water is dipole fluctuation which may help in explaining the actual spectral enlargement when polarity is increased. Most importantly, our results reproduce the effect of the perturbing environment on pyrene spectral intensities. This intriguing aspect deserves a deeper inspection. According to the definition of the molecular absorption coefficient as reported in the eqs 4 and 5, important information may be obtained by analyzing the values of the calculated perturbed transition dipole squared lengths, i.e., $|\boldsymbol{\mu}_{i,j}|^2$, in the different environments. For this purpose we report in Table 4 the deviation of mean perturbed $|\boldsymbol{\mu}_{i,j}|^2$ with respect to the corresponding unperturbed (gas phase) values, for the strongly allowed transitions, i.e., $S_0 \rightarrow S_2$ and $S_0 \rightarrow S_5$ for PMM-ZINDO and $S_0 \rightarrow S_1$ and $S_0 \rightarrow S_5$ for PMM-TD-DFT-B3LYP.

As expected from the results previously reported, i.e., Table 3, the values of Table 4 reveal a strong reduction of the transition dipole with respect to the unperturbed value on increasing the polarity of the medium. Note that pyrene is better solubilized in low polar medium and, therefore, it might be expected to preferentially reside in the hydrophobic compartment of membrane. These results, however, do not clearly solve the starting question as to why and to what extent the medium affects the transition intensity. An answer to this question may be provided by more accurately characterizing pyrene perturbed electronic states.[8]

Our analysis starts by considering the orthonormal set of electronic states of gaseous pyrene, i.e., the unperturbed Hamiltonian eigenvectors obtained by using quantum-chemical approaches such as ZINDO or TD-DFT, as a 13-dimensional space. Each unit vector of this space represents the ground, Φ_0^0, and the excited electronic states of pyrene in the lack of any external stimulus.

According to PMM procedure, along MD simulation each pyrene-perturbed electronic state (perturbed Hamiltonian eigenvector) is defined as a trajectory spanning the above 13-dimensional space, through the rotational fluctuation of a unit vector. The (sub)space of the electronic state space, where the eigenvector is mainly confined, can be identified by carrying out a principal-component analysis on each eigenvector trajectory.[8] This is performed by constructing the correlation matrix $\tilde{C}_i = \langle \mathbf{c}_i \mathbf{c}_i^{\mathrm{T}} \rangle$ for the i-th Hamiltonian eigenvector. Diagonalization of this matrix produces a set of eigenvectors, $\boldsymbol{\eta}_{l,i}$ which define the directions in the electronic state space maximizing/minimizing the Hamiltonian eigenvector mean square projection provided by the corresponding eigenvalue $\lambda_{l,i} = \langle |\boldsymbol{\eta}_{l,i}^{\mathrm{T}} \mathbf{c}_i|^2 \rangle$. The eigenvalue spectrum will therefore characterize the set of eigenvectors, i.e., the eigenvectors with values different from zero, to be used to describe the above unit vector rotation. Obviously, when only one eigenvector significantly differs from zero, no rotation occurs and the perturbed state, i.e., time-independent state, can be considered as a static unit vector. This analysis was then performed to characterize the pyrene-perturbed ground state (S_0) and the most relevant vertical transitions, i.e., states S_2 and S_5 according to PMM-ZINDO basis set. Note that results from PMM-TD-DFT-B3LYP produced the same picture and will therefore not be reported for the sake of brevity.

In Figure 3 we report the principal-component eigenvalues for S_0, S_2, and S_5 in the different investigated environments. The corresponding principal-component eigenvectors expressed in the unperturbed basis set are reported in Figure 4. Note that in both figures we have reported only the first seven states. From Figures 3 and 4 it is evident that S_0 can be entirely described by using only one principal-component eigenvector virtually coincident with the unperturbed electronic ground state; i.e., expression of the perturbed eigenvector in the unperturbed basis set shows only the first component basically equal to one. The S_2 state, i.e., the first intense vertical transition, behaves similarly to S_0; i.e., the perturbed S_2 coincides with unperturbed S_2 when methanol, POPC, and acetonitrile are considered. On the other hand, two principal-component eigenvectors significantly differing from zero are found for aqueous S_2, indicating a dynamic mixture of unperturbed S_1 and S_2.

This finding can be better appreciated by considering Figure 5 in which we report the distribution of projections of pyrene-perturbed S_2 eigenvector onto the plane defined by the first two

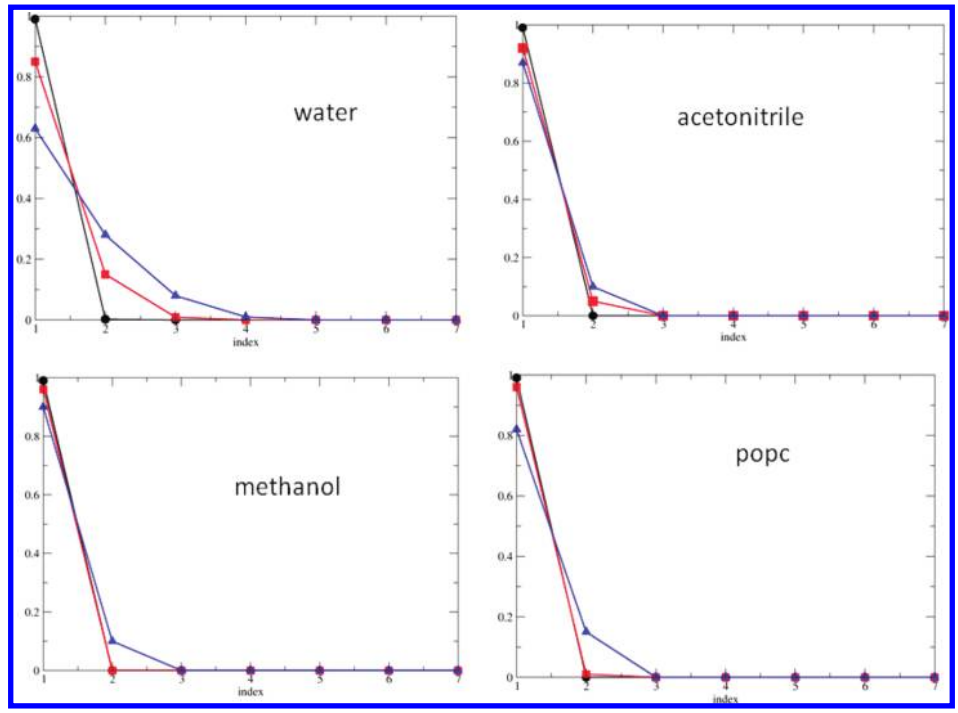

Figure 3. Principal-component eigenvalues for pyrene-perturbed S_0 (circles, black), S_2 (squares, red), and S_5 (triangles up, blue) states in the indicated environments. Note that in the abscissa are reported the index from 1 to 7 of covariance matrix eigenvectors.

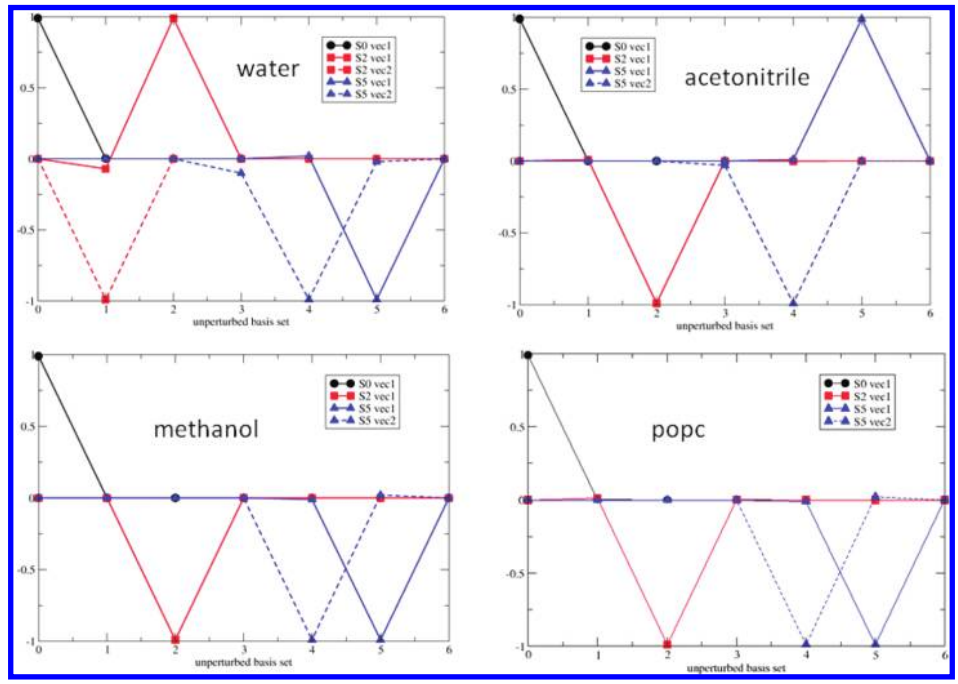

Figure 4. Relevant principal-component eigenvectors for pyrene-perturbed S_0 (circles, black) S_2 (squares, red), and S_5 (triangles up, blue) states in the indicated environments. Note that, whenever necessary, the second principal-component eigenvector (vec2) is represented with the dotted line. The unperturbed electronic states have been used as basis set. Note that in the abscissa the numbers from 0 to 6 refer to unperturbed ground and first six unperturbed excited states used as 13-dimensional basis set (see text).

principal-component eigenvectors, virtually coincident with unperturbed S_1 and S_2. In the case of aqueous S_2 we observe a sharp rotation of the unit vector indicating the cited dynamic mixture of the two states. Considering that S_1 state is essentially forbidden from S_0, i.e., very low $|\boldsymbol{\mu}_{i,j}|^2$, its relevant statistical weight in the description of perturbed S_2 produces the strong signal intensity reduction found for the first intense transition in water. Interestingly, fluctuation of unit vector around the zero of vec2, that is, the contamination of allowed state with the forbidden one, progressively reduces when we pass from water to acetonitrile, methanol, and POPC membrane. This basically parallels the progressive reduction of absorption intensity.

A further interesting aspect emerges from the analysis of pyrene in POPC reported in Figure 6. In this case we have monitored the projection of S_2 unit vector onto the second essential eigenvector, basically the unperturbed S_1 state (see Figures 3 and 4), as a function of the "z" quota within the POPC membrane. In other words, we have evaluated how much the perturbed S_2 state is "contaminated" by, i.e., projects onto, the unperturbed (forbidden) S_1 state in the different positions of

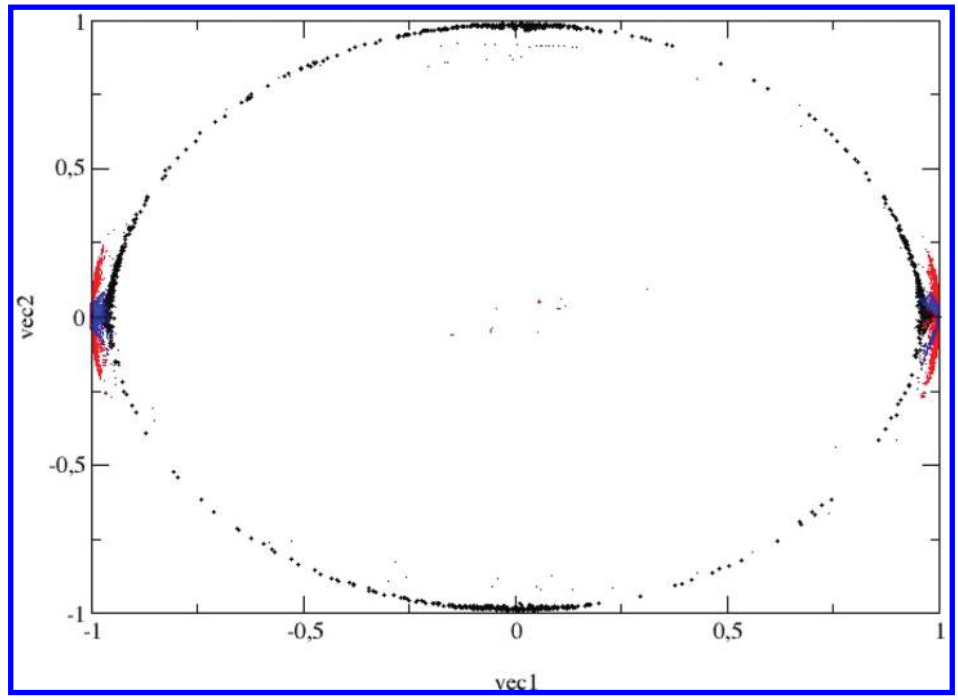

Figure 5. Projection distribution of S_2 state onto the plane defined by the relevant two principal-component eigenvectors for water (black), acetonitrile (red), and POPC bilayer (blue). Note that the projection distribution of S_2 state for methanol does not appear as it is overwhelmed by that of the POPC membrane.

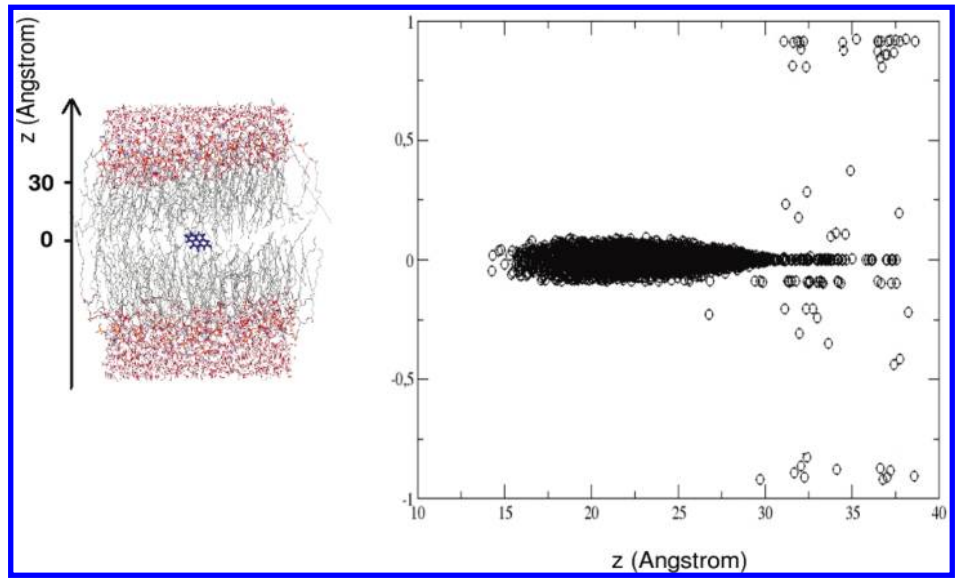

Figure 6. Projection of pyrene S_2 perturbed state onto the second essential eigenvector in POPC versus the quota (z) of the pyrene geometrical center along the simulation.

pyrene within the membrane. It can be easily observed that, when pyrene reaches the polar headgroup region, i.e., between 35 and 40 Å, it also undergoes the mixing between unperturbed S_1 and S_2 already observed in the aqueous environment and completely absent in the hydrophobic center of the membrane. This means that, when pyrene is confined within the hydrophobic reagion, its absorption intensity reaches the maximum values and undergoes a strong reduction in the polar region.

A slightly different picture is found when the S_5 state is considered. The related spectrum of eigenvalues suggests that a dynamic character, although much more pronounced in water, is present in all of the investigated environments. From inspection of eigenvectors it also emerges that in acetonitrile, methanol, and POPC bilayer perturbed S_5 rotates in the plane defined by unperturbed S_4 and S_5. On the other hand, in water a not negligible projection onto the unperturbed S_3 is observed.

The distribution of projections of pyrene-perturbed S_5 eigenvector onto the plane defined by the first two principal-component eigenvectors, virtually coincident with unperturbed S_4 and S_5, is reported in Figure 7. Differently from the situation reported in Figure 5, a dynamic character of the perturbed eigenvector can be observed also for nonaqueous solvents, suggesting a larger extent of the mixing. Note that a quantitatively significant population is also found in the center of the plane for aqueous S_5. This is due to the mentioned role of S_3 unperturbed eigenvector (see triangles in Figure 4). Obviously, the mixing of S_5 with the intrinsically less intense S_4 results in

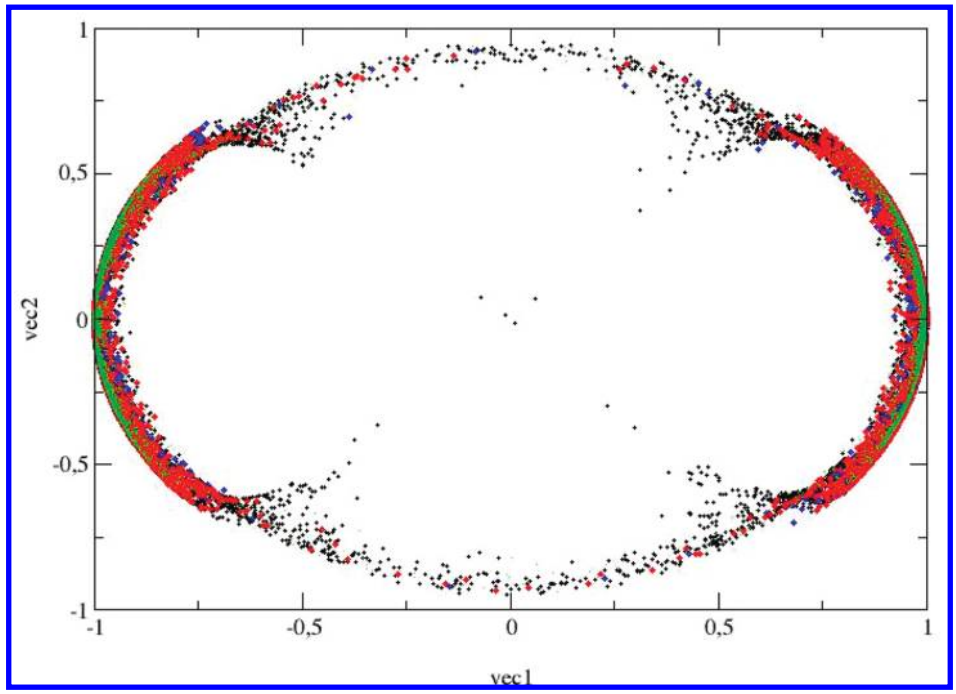

Figure 7. Projection distribution of S_5 state onto the plane defined by the relevant two principal-component eigenvectors for water (black), acetontrile (red), methanol (green), and POPC membrane (blue).

the differential peak intensity obtained for $S_0 \rightarrow S_5$ in the different solvents.

4.4. Evaluation of the Vibronic Structure of First Electronic Absorption Spectrum in Aqueous Pyrene. As a final step of our investigation, we addressed the modeling of the fine vibronic structure which characterizes pyrene absorption spectrum in aqueous solution. Note that we limited our analysis only to the first intense transition, namely S_0-S_2.

Vibronic structure in the condensed phase requires the possibility of evaluating perturbed vibrational eigenstates of a polyatomic system. This problem has been recently addressed in our laboratory and is described in detail in the literature.[48,49] Briefly, we assume that for typical quantum vibrational degrees of freedom the environment perturbation does not significantly alter the vibrational modes (i.e., the mass-weighted Hessian eigenvectors) but only produces variations of the Hessian eigenvalues. Therefore, once the unperturbed mass-weighted Hessian eigenvectors are defined by a gas-phase calculation on the pyrene, we may obtain ω^2 values at each QC-environment configuration via a quadratic fit to the perturbed electronic ground state energy calculated by PMM for each structure along the corresponding mode (unperturbed eigenvector). This procedure is revealed as rather efficient for reproducing electronic ground-state vibrational states.[49] In the case of vibronic structure, we need electronic excited-state frequencies. At this purpose, as far as low-energy excited electronic states are concerned, we may still consider valid the approximations adopted for electronic ground state. Therefore, applying the same procedure and using the electronic excited state mass-weighted Hessian eigenvectors, we may obtain the perturbed electronic excited state frequencies. In the case of pyrene, this application may be frustrated by the large number of vibrational dregrees of freedom. However, as already remarked in previous theoretical and experimental literature, the dominant transitions correspond to excitations of totally symmetric normal modes.[50−53] Therefore, we have limited our analysis to this subspace of harmonic oscillators. S_2 mass-weighted Hessian has been evaluated at the CIS/3-21G level of theory exactly reproducing already published data.[52] Five pyrene configurations were generated, through steps of 0.05 au along each of the 20 totally symmetric eigenvectors. On these structures we applied PMM at the ZINDO level of theory and the perturbed energies were used for the quadratic fit to provide the excited electronic state frequencies along the MD trajectory. The frequency distributions of the electronic excited state are shown in the Supporting Information. A rigorous treatment of vibronic spectrum evaluation would require the explicit calculation of the transition dipole moment for the vibronic excitations. As shown in the literature, this procedure, although not straightforward, has been successfully applied to gaseous pyrene[51] and, although more complicated in condensed phase, could be used also in aqueous pyrene by means of PMM calculations.[48] However, given the large number of vibrational-electronic states to be considered, in order to simplify the procedure we adopted the following assumptions: (i) only the strongly (electronic) dipole-allowed transitions have been considered in order to adopt the Franck−Condon approximation,[52] i.e., the electronic transition dipole to be integrated over the vibrational coordinates is approximated as a constant corresponding to the transition dipole value calculated in the correspondence of ground-state minimum; (ii) unperturbed (gas phase) intensities[51] have been rescaled by the ratio of the perturbed electronic transition dipole square length and the unperturbed transition dipole square length; and (iii) we neglect the possible difference in the zero-point vibrational energies between the electronic ground and excited state. Note that the latter assumption may be used to obtain the perturbed vibronic intensities when the vibrational frequency deviation due to the perturbation are small with respect to corresponding unperturbed frequencies, hence implying that the perturbed vibrational wave functions are virtually identical to the unperturbed ones. Such a condition is typically accomplished when we consider high-frequency modes as usual in our calculations.

The theoretical result shown in Figure 8 rather accurately reproduces the experimental 0−1 transition, although some differences emerge probably due to the approximations introduced to treat vibronic excitation in a simplified way. Such a

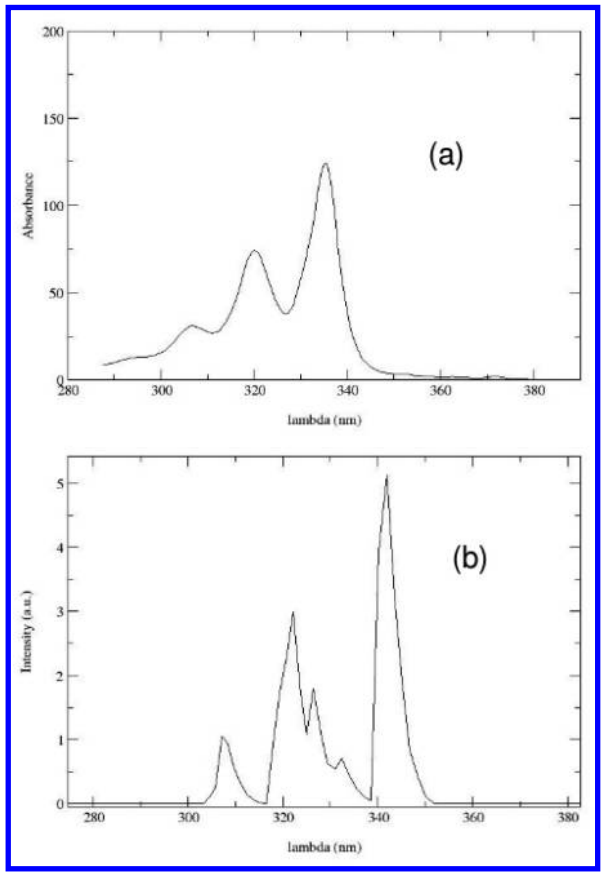

Figure 8. Experimental (a) and calculated (b) absorption spectrum of aqueous pyrene between 300 and 360 nm.

result, however, further confirms the rather good performance of the method providing a solid ground for the considerations outlined throughout the present study concerning the nature of perturbed quantum states in interacting molecular systems.

5. Conclusions

A systematic theoretical−experimental study has been carried out in order to obtain some information on the actual nature of perturbed singlet excited states of pyrene which represents a benchmark molecule for spectroscopists and theoreticians.[13] In particular, both absorption and emission intensities of this molecule, in particular concerning S_2 state, are known to be highly sensitive to the chemical nature of the surrounding environment. Experimental data confirm this trend and in particular evidence the tendency shown by pyrene to reduce the S_2 absorption intensity when the polarity of the medium is increased. Our theoretical analysis, based on a joint application of PMM and MD simulations and correctly reproducing pyrene vertical and vibronic spectral features, indicates that this phenomenon may be explained by representing perturbed electronic states in terms of statistical distribution in specific electronic subspace. In this way we have characterized for pyrene a clear correlation between the chemistry of the medium and the allowed fluctuations of the perturbed eigenstate in the electronic state space, providing the remarkable spectral variations observed. Such a behavior confirms the general features already observed for other chemical systems embedded in complex atomic−molecular environments[8] which provides a different viewpoint of the concept of electronic state in complex molecular environment.

Acknowledgment. The authors acknowledge CASPUR (Roma) for computational facilities and the use of Gaussian03.

Supporting Information Available: (1) Pyrene-optimized geometries used for quantum-chemical calculations; (2) atomic charges used for molecular dynamics simulations; (3) pyrene coordinates used for MD simulations; (4) analysis of the "*z*" quota spanned by pyrene in membrane from MD simulation; (5) perturbed total-symmetric frequencies of S_2 state of pyrene in water; (6) experimental spectra of pyrene in different solvents. This material is available free of charge via the Internet at http://pubs.acs.org.

References and Notes

(1) Martin, R. *Electronic Structure Basic Theory and Practical Methods*; Cambridge University Press: Cambridge, UK, 2004.
(2) Hung, L.; Carter, E. A. *Chem. Phys. Lett.* **2009**, *475*, 163.
(3) Aschi, M.; Spezia, R.; Di Nola, A.; Amadei, A. *Chem. Phys. Lett.* **2001**, *344*, 374.
(4) Amadei, A.; D'Abramo, M.; Zazza, C.; Aschi, M. *Chem. Phys. Lett.* **2003**, *381*, 187.
(5) Zazza, C.; Amadei, A.; Sanna, N.; Grandi, A.; Chillemi, G.; Di Nola, A.; D'Abramo, M.; Aschi, M. *Phys. Chem. Chem. Phys.* **2006**, *8*, 1385.
(6) Amadei, A.; D'Alessandro, M.; Aschi, M. *J. Phys. Chem. B* **2004**, *118*, 16250.
(7) Amadei, A.; Di Nola, A.; Aschi, M. In *Solvation Effects in Molecules and Biomolecules*; Canuto, S., Ed.; Springer: New York, 2008; p 191.
(8) Amadei, A.; D'Alessandro, M.; D'Abramo, M.; Aschi, M. *J. Chem. Phys.* **2009**, *130*, 084109.
(9) Cundall, R. B.; Pereira, E. A. *Chem. Phys. Lett.* **1973**, *18*, 371.
(10) Dong, D. C.; Winnik, M. A. *Can. J. Chem.* **1984**, *62*, 2560.
(11) Tucker, S. A.; Acree, W. E.; Street, K. W.; Fetzer, J. C.; John, C. *Appl. Spectrosc.* **1989**, *43*, 162.
(12) Chen, S. H.; McGuffin, V. L. *Appl. Spectrosc.* **1994**, *48*, 596.
(13) Basu Ray, G.; Chakraborty, I.; Moulik, S. P. *J. Colloid Interface Sci.* **2006**, *294*, 248–254.
(14) Karpovich, D. S.; Blanchard, G. J. *J. Phys. Chem.* **1995**, *99*, 3951.
(15) Waka, Y.; Mataga, N.; Tanaka, F. *Photochem. Photobiol.* **1980**, *32*, 335.
(16) De Maria, P.; Fontana, A.; Gasbarri, C.; Velluto, D. *Soft Matter* **2006**, *2*, 595.
(17) Berendsen, H. J. C.; Postma, J. P. M.; Van Gunsteren, W. F.; Hermans, J. In *Intermolecular Forces*; Pullman, B., Ed.; Reidel Publishing Co.: Dordrecht, The Netherlands, 1981.
(18) Grabuleda, X.; Jaime, C.; Kollman, P. A. *J. Comput. Chem.* **2000**, *21*, 901.
(19) Tieleman, D. P.; Forrest, L. R.; Sansom, M. S. P.; Berendsen, H. J. C. *Biochemistry* **1998**, *37*, 17554.
(20) Berger, H. J. C.; Edholm, O.; Jähnig, F. *Biophys. J.* **1997**, *71*, 2002.
(21) Amadei, A.; Chillemi, G.; Ceruso, M.; Grottesi, A.; Di Nola, A. *J. Chem. Phys.* **2000**, *112*, 9.
(22) Berendsen, H. J. C.; Postma, J. P. M.; Van Gunsteren, W. F.; Di Nola, A. *J. Chem. Phys.* **1984**, *81*, 3684.
(23) Hess, B.; Bekker, H.; Berendsen, H. J. C.; Frajie, J. G. E. M. *J. Comput. Chem.* **1997**, *18*, 1463.
(24) Darden, T. A.; York, D. M.; Pedersen, J. G. *J. Chem. Phys.* **1993**, *98*, 10089.
(25) Van Gunsteren, W. F.; Billeter, S. R.; Eising, A. A.; Hunemberger, P. H.; Kruger, P.; Mark, A. E. Scott, V. R. P.; Tironi, I. G. *Biomolecular simulation: The GROMOS96 manual and user guide*; Hochschlverlag AG an der ETH: Zurich, 1996.
(26) Breneman, C. M.; Wiberg, K. B. *J. Comput. Chem.* **1990**, *11*, 361.
(27) Parr, R. G.; Yang, W. *Density functional theory of atoms and molecules*; Oxford University Press: New York, 1999.
(28) Becke, A. D. *J. Chem. Phys.* **1993**, *98*, 5648.
(29) Frisch, M. J.; Trucks, G. W.; Schlegel, H. B.; Scuseria, G. E.; Robb, M. A.; Cheeseman, J. R.; Montgomery, Jr., J. A.; Vreven, T.; Kudin, K. N.; Burant, J. C.; Millam, J. M.; Iyengar, S. S.; Tomasi, J.; Barone, V.; Mennucci, B.; Cossi, M.; Scalmani, G.; Rega, N.; Petersson, G. A.; Nakatsuji, H.; Hada, M.; Ehara, M.; Toyota, K.; Fukuda, K.; Hasegawa, J.; Ishida, M.; Nakajima, T.; Honda, Y.; Kitao, O.; Nakai, H.; Klene, M.; Li, X.; Knox, J. E.; Hratchian, H. P.; Cross, J. B.; Adamo, C.; Jaramillo, J.; Gomperts, R.; Stratmann, R. E.; Yazyev, O.; Austin, A. J.; Cammi, R.; Pomelli, C.; Ochterski, J. W.; Ayala, P. Y.; Morokuma, K.; Voth, G. A.; Salvador, P.; Dannenberg, J. J.; Zakrzewski, V. G.; Dapprich, S.; Daniels, A. D.; Strain, M. C.; Farkas, O.; Malick, D. K.; Rabuck, A. D.; Raghavachari, K.; Foresman, J. B.; Ortiz, J. V.; Cui, Q.; Baboul, A. G.; Clifford, S.; Cioslowski, J.; Stefanov, B. B.; Liu, G.; Liashenko; Piskorz, P.; Komaromi, I.; Martin, R. L.; Fox, D. J.; Keith, T.; Al-Laham, M. A.; Peng, C. Y.; Nanayakkara, A.; Challacombe, M.; Gill, P. M. W.; Johnson,

B.; Chen, W.; Wong, M. W.; Gonzalez, C.; Pople, J. A. *Gaussian 03, Revision C.01*; Gaussian, Inc.: Wallingford, CT, 2004.

(30) Schmidt, M. W.; Baldridge, K. K.; Boatz, J. A.; Elbert, S. T.; Gordon, M. S.; Jensen, J. H.; Koseki, S.; Matsunaga, N.; Nguyen, K. A.; Su, S. J.; Windus, T. L.; Dupuis, M.; Montgomery, J. A. *J. Comput. Chem.* **1993**, *14*, 1347.

(31) Ferguson, J.; Reeves, L. W.; Schneider, W. G. *Can. J. Chem.* **1957**, *35*, 1117.

(32) Salvi, P. R.; Foggi, P.; Castellucci, F. *Chem. Phys. Lett.* **1983**, *98*, 206.

(33) Azumi, T.; McGlynn, S. P. *J. Chem. Phys.* **1964**, *41*, 3131.

(34) Bito, Y.; Shida, N.; Toru, T. *Chem. Phys. Lett.* **2000**, *328*, 310.

(35) Park, Y. H.; Cheong, B.-S. *Curr. Appl. Phys.* **2006**, *6*, 700.

(36) Tuan, V. D.; Wild, U. P.; Lamotte, M.; Merle, A. M. *Chem. Phys. Lett.* **1976**, *39*, 118.

(37) Voityuk, A. A.; Zerner, M. C.; Rosch, N. *J. Phys. Chem. A* **1999**, *103*, 4553.

(38) Wang, B.-C.; Chang, J.-C.; Tso, H.-C.; Hsu, H.-F.; Cheng, C.-H. *J. Mol. Struct. (THEOCHEM)* **2003**, *629*, 11.

(39) Gross, E. K. U.; Dobson, J. F.; Petersilka, M. In *Density Functional Theory II*; Nalewajski, R. F., Ed.; Springer: Heidelberg, Germany, 1996; Springer Series in Topics in Current Chemistry, Band 181.

(40) Parac, M.; Grimme, S. *Chem. Phys.* **2003**, *292*, 11.

(41) Perdew, P.; Burke, K.; Ernzerhof, M. *Phys. Rev. Lett.* **1996**, *77*, 3865.

(42) Van Voorhis, T.; Scuseria, G. E. *J. Chem. Phys.* **1998**, *109*, 400.

(43) Piecuch, M.; Kucharski, S. A.; Kowalski, K.; Musial, M. *Comput. Phys. Commun.* **2002**, *149*, 71.

(44) Becker, R. S.; Singh, I. S.; Jackson, E. A. *J. Chem. Phys.* **1963**, *38*, 2144.

(45) Khakhel, O. A. *J. Appl. Spectrosc.* **2001**, *68*, 280.

(46) Perochon, E.; Lopez, A.; Tocanne, J. F. *Biochemistry* **1992**, *31*, 7672.

(47) Blatt, E.; Launikonis, A. L.; Mau, A. W.-H.; Sasse, W. H. F. *Aust. J. Chem.* **1987**, *40*, 1.

(48) Amadei, A.; Marinelli, F.; D'Abramo, M.; D'Alessandro, M.; Anselmi, M.; Di Nola, A.; Aschi, M. *J. Chem. Phys.* **2005**, *122*, 124506.

(49) Amadei, A.; Aschi, M. *IJLSS* 2009, in press.

(50) Borisevich, N. A.; Vodovatov, L. B.; D'yachenko, G. G.; Petukhov, V. A.; Semyonov, M. A. *J. Appl. Spectrosc.* **1995**, *62*, 482.

(51) Dierksen, M.; Grimme, S. *J. Chem. Phys.* **2004**, *120*, 3544.

(52) Goodpaster, J. V.; Harrison, J. F.; McGuffin, V. L. *J. Phys. Chem. A,* **1998**, *102*, 3372.

(53) Atkins, P. W.; Friedman, R. S. *Molecular Quantum Mechanics*, 3rd ed.; Oxford University Press: New York, 1997.

JP909465F